

Continuous-wave and pulsed EPR studies of Cr^{2+} defects in CaF_2

P. B. Oliete, V. M. Orera, and P. J. Alonso

Instituto de Ciencia de Materiales de Aragón, Consejo Superior de Investigaciones Científicas, Universidad de Zaragoza, Pza. San Francisco s/n, E-50009 Zaragoza, Spain

(Received 1 August 1995)

Cr_2O_3 and CrF_3 doped CaF_2 single crystals have been studied by cw-EPR and electron spin echo envelope modulation (ESEEM) techniques. In both cases Cr^{2+} ions enter the fluorite structure at substitutionally distorted cation sites. For Cr_2O_3 doped crystals, X and Q band EPR measurements at temperatures between 4 and 200 K allowed us to determine the ion symmetry and spin Hamiltonian parameters, such as the g factors and the zero-field splitting tensors, as well as the $^{53}\text{Cr}^{2+}$ hyperfine tensor. Electron spin echoes (ESE) were detected on that system at temperatures below 20 K. The analysis of the ESEEM and cw-EPR superhyperfine (shf) structure lead us to propose a model composed of two nearest-neighbor fluoride ions placed in the (110) plane containing the C_2 axis with the ones opposite substituted by an O^{2-} ion. For CrF_3 doped crystals the distortion is also orthorhombic but the shf interaction is with four fluoride ions presumably in the (110) plane perpendicular to the z defect axis. No ESE was detected for this system. A linewidth narrowing effect was observed. We assign this distortion to a dynamical Jahn-Teller effect corresponding to $T_{2g} \otimes (t_g + e_g)$ coupling stabilized by lattice stresses.

I. INTRODUCTION

The Jahn-Teller effect (JT) occurs in ions with orbitally degenerate ground states as a consequence of the coupling of the electronic states with some lattice modes.¹ The JT theorem² states that for electronically degenerate molecules or ions in a solid, a distortion exists which reduces the symmetry of the system. In spite of the tremendous amount of theoretical and experimental work performed in this area since its discovery sixty years ago, there are still some aspects of the electron-phonon coupling which are not fully understood.

In particular, some uncertainties exist about the expected (JT) distortion for orbital triplet states in cubic systems. In fact, as first discussed by Van Vleck³ and more extensively by Opik and Pryce,⁴ linear coupling to e and t_2 modes only predicts two types of distortion, tetragonal or trigonal according to the relative strength between e and t_2 couplings, whereas there is little experimental evidence for orthorhombic JT distortions.

Let us consider the case of Cr^{2+} ions (d^4). Since this configuration is non-Kramers, very few EPR studies are available. For tetrahedral and cubic symmetry, the ground state is the orbital triplet $^5T_{2(g)}$. Usually in tetrahedral environments the orbital degeneracy is lifted by a tetragonal JT distortion, as has been observed for cubic ZnS , ZnSe , ZnTe , and CdTe crystals⁵ by a clear indication of the predominance of $T \otimes e$ JT coupling in these compounds. On the other hand, for $\text{CdF}_2:\text{Cr}$ (Ref. 6) and $\text{SrF}_2:\text{Cr}$,⁷ which to our knowledge are the only cubic Cr^{2+} systems studied to date, the distortion is orthorhombic.

It is interesting to note that, although not predicted by linear JT theory, several authors (Bacci *et al.*,⁸ Sakamoto,⁹ Estreicher and Estle,¹⁰ and others) have shown that for O_h symmetry clusters, orthorhombic distortions are possible when simultaneous coupling to e_g and t_{2g} modes and quadratic or bilinear coupling terms and/or anharmonic potential

terms are included in the electron-lattice Hamiltonian. In this case the number of different coupling constants is large and in practice the Hamiltonian has to be solved numerically for each particular case, which makes it difficult to know *a priori* the magnitude of the distortion expected for a given system. We therefore have to rely on experiments, with electron paramagnetic resonance (EPR) being one of the best tools since it can provide information on the ion ground state and environment.

The question now becomes is Cr^{2+} orthorhombic distortion, as found for CdF_2 and SrF_2 , a general trend through all the fluorite series?¹¹ We have, therefore, undertaken the study of the Cr^{2+} ion in the alkaline-earth halides by the EPR technique to obtain models for the different systems, as well as useful experimental parameters such as g factors, zero-field splitting and cubic field parameters, hyperfine and superhyperfine constants. We have found tetragonally distorted Cr^{2+} ions for BaF_2 and SrCl_2 (Ref. 12) and corroborated the orthorhombic symmetry for SrF_2 recently proposed by Zari-pov *et al.*⁷ Here we present the results for CaF_2 .

The first problem to deal with concerns the reliability of the assignment of the distortions given by to a JT effect. In fact, most of the $3d$ ions in ionic matrices show EPR spectra with conventional line shapes. The usual absence of any dynamical effect makes it difficult to distinguish between a true JT effect or a perturbation due to foreign atoms or lattice point defects. For example, in an old work on CaF_2 doped with $3d$ ions some evidence was given for the existence of orthorhombic Cr^{2+} ions interacting with two fluoride ions.¹³ In the fluorite lattice this defect structure is very unlikely for unperturbed substitutional ions.

In the present work we prove that doping with either chromium oxide or fluoride produces different orthorhombic distorted substitutional Cr^{2+} centers, $\text{Cr}^{2+}(\text{I})$, and $\text{Cr}^{2+}(\text{II})$ with a superhyperfine (shf) interaction with two and four fluoride ions, respectively, the latter being presumably the true unperturbed JT distorted defect and the former being associated

with oxygen impurities. Electron spin echo (ESE) is detected for the $\text{Cr}^{2+}(\text{I})$ system thus allowing us to study the super-hyperfine interaction with the surrounding fluoride ions by analyzing the electron spin echo envelope modulation (ESEEM) signal.

II. EXPERIMENTAL DETAILS

Single CaF_2 crystals doped with CrF_3 used in this study were grown in our laboratory using a standard Bridgman method. The CrF_3 content in the starting materials was 0.5%. Single CaF_2 crystals doped with Cr_2O_3 were provided by den Hartog ranging from 0.1 to 1% Cr_2O_3 content. Both samples were colorless.

X-band EPR measurements were performed using either a Bruker ESP-380E or a Varian E-112 spectrometer. Q -band EPR and ESEEM measurements were performed with a Bruker ESP-380E. Liquid-nitrogen temperature (LNT) measurements were taken using an immersion quartz dewar and the low temperature measurements were made using an Oxford CF 100 and CF 935 continuous flow cryostat. A Varian E-257 continuous flow cryostat was used for measurements between LNT and 300 K. Magnetic field values were determined with a NMR gaussmeter. The diphenylpicrylhydrazyl (DPPH) signal ($g=2.0037\pm 0.0002$) for the Q band and a Hewlett-Packard microwave frequency counter 5350B were used to measure the microwave frequency.

III. EXPERIMENTAL RESULTS AND INTERPRETATION

First we wish to point out that the analysis of the EPR spectra is somewhat complicated by crystal field terms of a strength comparable to the Zeeman term and also by super-hyperfine constants of the same magnitude as the nuclear Zeeman interaction. In these cases, measurements at different microwave frequencies were necessary.

We have measured the EPR spectra of $\text{CaF}_2:\text{Cr}$ crystals doped with Cr_2O_3 and CrF_3 in the X and Q bands as a function of the angle between the crystallographic axes and the external magnetic field \mathbf{B} at temperatures in the 4–200 K range. In both cases we obtained an anisotropic spectrum corresponding to an ion with an electronic spin of 2 and an orthorhombic symmetry that we assigned to Cr^{2+} . Two different defects, $\text{Cr}^{2+}(\text{I})$ and $\text{Cr}^{2+}(\text{II})$, are obtained depending on the doping salt (Cr_2O_3 and CrF_3 , respectively). The angular dependence of the resonance lines, positions, and intensities can be explained by the following approximate spin Hamiltonian (SH) for orthorhombic symmetry:

$$\hat{H} = \beta(g_x S_x B_x + g_y S_y B_y + g_z S_z B_z) + D S_z^2 + E(S_x^2 - S_y^2) + \frac{1}{6} a(S_1^4 + S_2^4 + S_3^4) + \frac{1}{180} F(35S_z^4 - 15S_z^2), \quad (1)$$

with $S=2$ and $x=[\bar{1}10]$, $y=[001]$, and $z=[110]$.

In Eq. (1) the SH parameters have their usual meaning. In the cubic a term, 1, 2, and 3 are the axes of the cube. The F term in Eq. (1) is small and the spectra are rather insensitive to this parameter. We have assumed F to be zero throughout the analyses.

For both cases, the dominant fine structure term is D , which produces a splitting of the fivefold spin degenerated

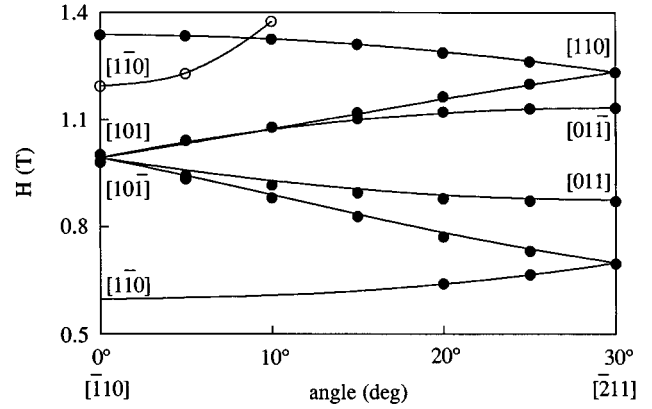


FIG. 1. The angular dependence of the EPR line positions of $\text{CaF}_2:\text{Cr}^{2+}(\text{I})$ measured in the (111) plane at 77 K in the Q band. Transitions are labeled with their distortion z axis. The experimental points correspond to \circ : $|0\rangle \leftrightarrow |+1\rangle$ and \bullet : $|+1\rangle \leftrightarrow |-1\rangle$ transitions. Solid lines give the computed line positions using Eq. (1) and the parameter value given in the text.

state into a singlet ($M_s=0$) and two doublets ($M_s=\pm 1$ and $M_s=\pm 2$) at a distance at zero field of $\approx D$ and $4D$, respectively. The observed spectrum depends strongly upon the size of D relative to the microwave energy $h\nu_0$.

In the X band ($|D| \gg h\nu_0$) we can only observe the forbidden $|+1\rangle \leftrightarrow |-1\rangle$ and $|+2\rangle \leftrightarrow |-2\rangle$ transitions, the intensity of the latter being proportional to a^2 , whereas in the Q band ($|D| \approx h\nu_0$) the allowed $|0\rangle \leftrightarrow |\pm 1\rangle$ transition can also be observed. The sign of D was determined using the temperature dependence of the line intensities in the range 4–35 K.

A. $\text{CaF}_2:\text{Cr}^{2+}(\text{I})$

Measurements were performed in the (100), (110), and (111) planes at 9.3 and 34 GHz. As an example the angular dependence for a (111) plane in the Q band is given in Fig. 1. It corresponds to an orthorhombic defect whose principal axes are the ones defined above. For this plane the six defects are observed. In the $[110]$ direction, the high field signal (≈ 1338 mT) corresponds to the magnetic field along the defect x axis while the low field one (≈ 600 mT) corresponds to the $z \parallel \mathbf{B}$ center. The solid lines represent the calculated line positions using an exact diagonalization of Eq. (1), with the following values of the parameters:

$$g_{\parallel} = 1.965(7), \quad g_{\perp} = 1.995(3),$$

$$D = -2.237(5) \text{ cm}^{-1}, \quad E = 0.0476(1) \text{ cm}^{-1}.$$

Excellent agreement with the observed positions is found. The transitions are labeled by their high field M_s values.¹⁴ It is interesting to note that the $|0\rangle \leftrightarrow |+1\rangle$ transition is also observed.

It can be seen that the departure from axial symmetry is very small ($E/D \ll 1$) and within the experimental error limits $g_x = g_y = g_{\perp}$. In agreement with intensity calculations using the eigenstates which diagonalize Eq. (1), the transition intensity decreases from high field to low field, vanishing when the defect z axis is parallel to the magnetic field. The rotational diagrams in the other planes and in the X band and

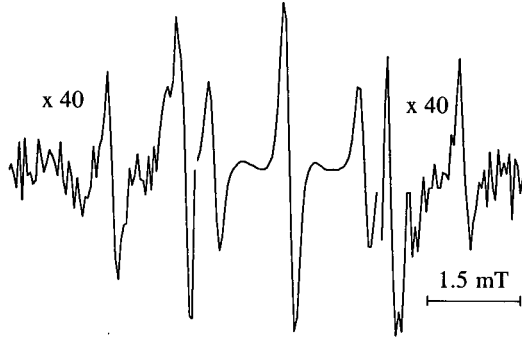


FIG. 2. The X-band spectrum of CaF₂:Cr²⁺(I) corresponding to the high field $|+1\rangle \leftrightarrow |-1\rangle$ transition measured at 77 K with the magnetic field along the [110] direction.

the line intensities are also in agreement with the defect symmetry and SH parameters given above.

The $|+2\rangle \leftrightarrow |-2\rangle$ transition is not observed for this compound, indicating that the a -term contribution is negligible. The sign of D was determined from the temperature dependence of the $|+1\rangle \leftrightarrow |-1\rangle$ line intensity at low temperatures. The D and E parameters are slightly dependent on temperature, with D increasing and E decreasing as the temperature decreases. In contrast to semiconductors, where the Cr²⁺ EPR signals decrease below detection limits at temperatures above 20 K,^{5,15} measurements can be performed up to 200 K.

Hyperfine (hf) structure

The X-band high field $|+1\rangle \leftrightarrow |-1\rangle$ spectrum for $\mathbf{B} \parallel [110]$ measured at 77 K is shown in Fig. 2. The peak to peak linewidth is 0.2 mT at this temperature and increases as the temperature increases. Above 240 K the lines are so broad that they cannot be resolved. The central structure consists of three lines with an intensity ratio of 1:2:1 which can be associated with the shf interaction with two equivalent fluoride ions. On each side of these resonances, a pair of lines can be observed, which are about 40 times weaker than the central one. They are a replica of the central group where one line is not observed due to overlap with the stronger structure and are explained by the hf interaction with the 9.5% naturally abundant ⁵³Cr isotope ($I=3/2$). Of the four predicted hf resonances, the two inner ones are covered by the intense central group and cannot be observed. The measured splitting between the lines is 47.15 MHz. The same structure is observed in the Q band but with a different splitting (54.5 MHz).

In order to explain the hf spectrum the following axial hyperfine SH has been added to that given in Eq. (1):

$$\hat{H}_{\text{hf}} = A_{\parallel}({}^{53}\text{Cr})S_zI_z + A_{\perp}({}^{53}\text{Cr})(S_xI_x + S_yI_y), \quad (2)$$

where the parallel hf axis is chosen to be the defect z axis (see below). The hyperfine parameters were obtained by applying perturbation methods up to first order as follows.

For $\mathbf{B} \parallel [110]$ and perpendicular to the defect z axis, the expected values of the spin operators are $\langle S_y \rangle = \langle S_z \rangle = 0$ for the two electronic eigenstates involved in the transition (1 and 2) and the effective hf splitting (the measured splitting) is

$$A_{\text{eff}} = \pm (\langle S_x \rangle_1 - \langle S_x \rangle_2) A_{\perp} ({}^{53}\text{Cr}). \quad (3)$$

Thus A_{eff} depends on the microwave frequency as do the electronic eigenstates. Using the eigenstates of the SH given in Eq. (1) we have calculated $\langle S_x \rangle_1$ and $\langle S_x \rangle_2$ for both X and Q -band frequencies and thus obtained $A_{\perp}({}^{53}\text{Cr}) = 33.5 \pm 3$ MHz.

When the magnetic field is applied in the [001] direction and perpendicular to the defect z axis the mean values are $\langle S_x \rangle = \langle S_z \rangle = 0$ and A_{eff} is 11.4 and 46.5 MHz for the X and Q bands, respectively. A_{eff} related to the perpendicular hf parameter by

$$A_{\text{eff}} = \pm (\langle S_y \rangle_1 - \langle S_y \rangle_2) A_{\perp} ({}^{53}\text{Cr}). \quad (4)$$

Following the same procedure as above we obtained $A_{\perp}({}^{53}\text{Cr}) = 33.3 \pm 3$ MHz. The isotropy of the perpendicular hf parameter justifies the axis choice for H_{hf} .

For this orientation ($\mathbf{B} \parallel [001]$) the spectrum of the nonperpendicular defect shows two resolved replica that allow us to estimate $A_{\parallel}({}^{53}\text{Cr})$. In this case $\langle S_y \rangle = 0$ and the measured hf splitting is

$$A_{\text{eff}} = [(\langle S_x \rangle_1)^2 A_{\perp}({}^{53}\text{Cr})^2 + (\langle S_z \rangle_1)^2 A_{\parallel}({}^{53}\text{Cr})^2]^{1/2} + [(\langle S_x \rangle_2)^2 A_{\perp}({}^{53}\text{Cr})^2 + (\langle S_z \rangle_2)^2 A_{\parallel}({}^{53}\text{Cr})^2]^{1/2}. \quad (5)$$

The obtained value for the parallel hyperfine parameter $A_{\parallel}({}^{53}\text{Cr})$ is 36 ± 4 MHz.

shf structure

When the magnetic field is applied parallel to either the x or y defect axis, the EPR spectrum shows a three line structure with an intensity ratio of 1:2:1 in both the X and Q bands. If the field is applied in other directions, new lines appear and the pattern is different when measured in either the X or Q band.

As an example, the angular evolution of this structure in the (010) plane measured in the Q band at 77 K is shown in Fig. 3. The transitions correspond to the defect whose z axis is perpendicular to the [010] direction. The 1:2:1 intensity ratio can be explained by the superhyperfine interaction of the Cr²⁺ 3d electrons with two fluoride nuclei. At first sight, the other lines that appear, when the magnetic field is not in the [100] or [101] directions, could be assigned to the interaction with four crystallographically equivalent neighbor fluoride ions, as has been proposed by Jablonski¹⁶ and Zaripov⁷ in the case of chromium doped CdF₂ and SrF₂. However, with this model it is impossible to explain the different shf angular evolution observed in the X and Q band.

These experiments can be fully explained by a shf interaction with only two equivalent fluoride nuclei, the nuclear Zeeman term of fluorine is high and of a magnitude comparable to the shf term, the other lines being forbidden nuclear transitions. Thus up to nine transitions can be observed with a transition probability that depends on the nuclear eigenstate mixture.

To understand better this phenomenon, Fig. 4 shows an energy level diagram corresponding to the two extreme situations of parallel and perpendicular defects given in Fig. 3. When the defect is perpendicular, the resonance appears at high magnetic field values and the fluorine nuclear Zeeman terms are the dominant ones. The “allowed” transitions are

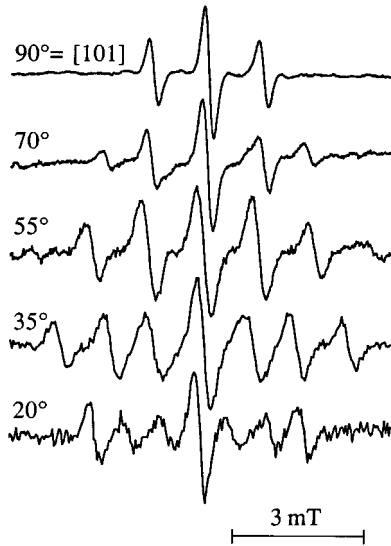


FIG. 3. The $|+1\rangle \leftrightarrow |-1\rangle$ Q -band spectrum of the $z||[10\bar{1}]$ defect, measured at 77 K when rotated in the (010) plane as a function of the angle between the defect z axis and the magnetic field. The intensities have been normalized to that of the central line.

now “nuclear transitions” and three lines with a 1:2:1 intensity ratio are observed. When the magnetic field is applied along the defect z axis, the resonance field reaches its lowest value and the allowed transitions are the outer “superhyperfine lines.” The differences between the X and Q -band spectra are now easily understood in terms of their different Zeeman nuclear contributions and of the different electronic eigenstates.

For this rotation plane, the EPR lines corresponding to the other four defects with z axes out of the (010) plane are doubly degenerate. Slight plane misalignment and line overlapping effects make the interpretation of the shf structure difficult in most cases. Thus we have used another technique with higher spectral resolution to solve the problem.

ESEEM experiments

Two pulses ($\pi/2-\tau-\pi$) and three pulses ($\pi/2-\tau-\pi/2-T-\pi/2$) experiments were performed in $\text{CaF}_2:\text{Cr}^{2+}(\text{I})$. Depending on

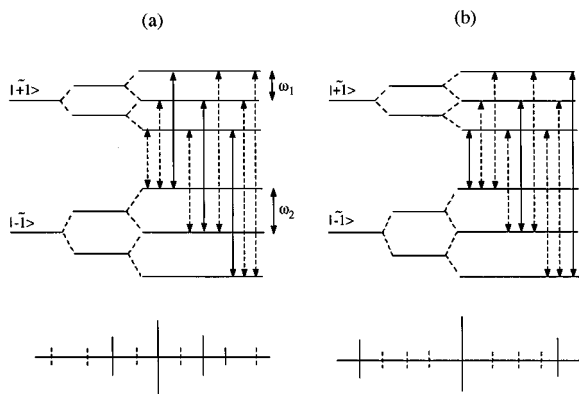


FIG. 4. The nuclear energy level diagram for two equivalent fluorine nuclei for the magnetic field being (a) perpendicular or (b) parallel to the defect axis. Solid lines represent the allowed transitions and dashed lines the forbidden transitions.

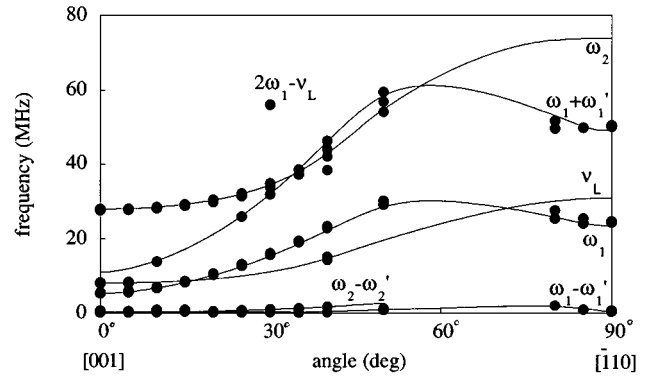


FIG. 5. The ESEEM three pulse experiment: angular dependence for $\text{Cr}^{2+}(\text{I})$ in the (110) plane at 9.8 GHz. ω_1 and ω_2 correspond to the energy between the nuclear levels in the up and down spin variety. ν_L is the fluorine Larmor frequency for the actual EPR resonance field. The points correspond to the experimental frequencies and the lines to the calculated ones using Eq. (6) and the values given in the text.

the experiment being of two or three pulses the decay time is T_M or T_1 , respectively. A periodic modulation of the echo amplitude is sometimes observed (ESEEM).¹⁷ The peaks obtained from the Fourier transformation (FT) of this modulation coincide with the electron nuclear double resonance (ENDOR) frequencies (ω_1 and ω_2 in Fig. 4) and their combinations. In the case of a three pulse experiment only the combination of the frequencies belonging to the same spin variety can be observed. In a two pulse experiment we can observe combinations between frequencies from different spin varieties ($\omega_1 \pm \omega_2$).

Spin echo was detected for the $|+1\rangle \leftrightarrow |-1\rangle$ EPR transitions at temperatures below 20 K. We have mainly studied results from the three-pulse experiment (stimulated echo) because they are simpler to analyze. In Fig. 5 we present the angular dependence, in the (110) plane, of the peaks obtained by FT analysis of the echo decays for the $|+1\rangle \leftrightarrow |-1\rangle$ EPR transition corresponding to the defect with the z -axis perpendicular to the rotation plane.

In this experiment the shf splittings of each spin level ω_1 and ω_2 are directly obtained. Due to a small rotation plane misalignment the two fluoride ions are slightly inequivalent and a splitting between the otherwise degenerate levels is detected.

Combining these ESEEM experiments with the cw-EPR shf measurements we mentioned above, we can propose the model given in Fig. 6. The model consists of two nearest-neighbor fluoride ions lying in the $(\bar{1}10)$ plane containing the defect z axis approximately along a $[111]$ direction.

To obtain the shf interaction constants and the position of the fluoride ions we have added the following SH to Eq. (1):

$$\hat{H}_{\text{shf}+nz} = \sum_i \{ -g_n \beta_n \mathbf{I}^i \mathbf{B} + \mathbf{S} \hat{\mathbf{A}}^i \mathbf{I}^i \}, \quad (6)$$

with $i=1,2$ which includes both nuclear Zeeman and superhyperfine terms. The latter is assumed to be axial along the $\text{Cr}^{2+}-\text{F}^-$ bond. In agreement with the angular dependence of the shf structure, we have chosen the shf axes x' , y' , and z' shown in Fig. 6 with $x' \parallel x$ and z' at an angle θ from the $[110]$

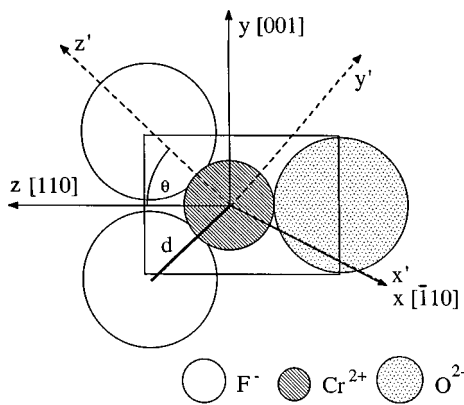


FIG. 6. The $\text{Cr}^{2+}(\text{I})$ defect model for CaF_2 . x, y, z are the defect axes and x', y', z' are the shf interaction axes.

direction. The eigenstates and eigenvalues of $H_{\text{shf}+nz}$ were found using the same first order perturbation method as indicated in the previous section. Fitting the experimental results we obtain $\theta = 44 \pm 5^\circ$, $A_{\parallel}^{\text{shf}(\text{I})} = +66 \pm 4$ MHz and $A_{\perp}^{\text{shf}(\text{I})} = +36 \pm 2$ MHz. Using these data we can reproduce the shf structure in all the directions studied so as the ESEEM results.

B. $\text{CaF}_2:\text{Cr}^{2+}(\text{II})$

The EPR of CaF_2 crystals doped with CrF_3 was measured at 9.8 and 34 GHz in the (100), (110), and (111) planes. In general the lines are much broader than for $\text{Cr}^{2+}(\text{I})$. In Fig. 7 the angular dependence of the resonance peaks in the (110) plane at 34 GHz is shown. Only the $|+1\rangle \leftrightarrow |-1\rangle$ and $|+2\rangle \leftrightarrow |-2\rangle$ transitions are observed in this case at this frequency. For the $|+1\rangle \leftrightarrow |-1\rangle$ transition the six centers corresponding to the orthorhombic symmetry are detected, some of them being equivalent in this plane. We could not observe the $|0\rangle \leftrightarrow |+1\rangle$ transition due to the experimental limits ($|\mathbf{B}| < 1.5$ T).

At 9.8 GHz we could only detect the $|+2\rangle \leftrightarrow |-2\rangle$ transitions, their field positions being almost proportional to $(1/\cos \theta)$ with θ the angle between the defect z axis (one of

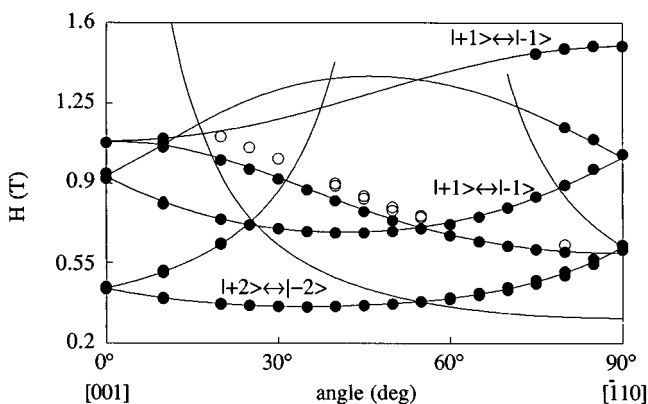


FIG. 7. The angular dependence for $\text{Cr}^{2+}(\text{II})$ in the (110) plane at 34 GHz. The circles are the experimental points and the lines the theoretical positions using the parameter values given in the text.

the six $[110]$ directions) and the direction of the magnetic field. A resonance peak at 920 mT is observed in the $[110]$ direction. We assign this line to the perpendicular $|+1\rangle \leftrightarrow |-1\rangle$ transition but the line broadens when we move out of this direction preventing us from studying its angular dependence. Above 40 K no signals are detected.

With only the $|+2\rangle \leftrightarrow |-2\rangle$ and $|+1\rangle \leftrightarrow |-1\rangle$ transitions it is not possible to obtain all the SH parameters from the fitting of Eq. (1) to the line positions. Thus we have used the following strategy: the sign and approximate value of D was obtained by fitting the Boltzmann statistic level population law to the temperature dependence of the $|+2\rangle \leftrightarrow |-2\rangle$ line intensity. The $|a|$ value was obtained from the ratio between the line intensities of the $|+1\rangle \leftrightarrow |-1\rangle$ and $|+2\rangle \leftrightarrow |-2\rangle$ transitions at 34 GHz measured in the $[100]$ direction. From this ratio we can only estimate the absolute value of a . Depending on its sign we obtain two different E values, namely 0.045 cm^{-1} if $a < 0$ and 0.07 cm^{-1} if $a > 0$. Some $|+1\rangle \leftrightarrow |-1\rangle$ resonances are expected to appear at 9.8 GHz thus explaining the resonance of 920 mT. Other $|+1\rangle \leftrightarrow |-1\rangle$ transitions should also appear but we have observed none of them. A possible explanation is that the line positions of these resonances are strongly dependent on the E value. That is because the zero field splitting of the $|\pm 1\rangle$ doublet is proportional to E . In consequence, a relatively narrow distribution of orthorhombic distortions can produce a very broad spread in the line positions and lead to an inhomogeneous broadening of these lines out of all recognition. The same effect explains the broadening of the $|+1\rangle \leftrightarrow |-1\rangle$ lines with respect to the $|+2\rangle \leftrightarrow |-2\rangle$ ones in the Q band. Of course the effect of the E distribution on the half-width of the latter is almost negligible since the zero-field splitting of the $|\pm 2\rangle$ level is in a first order approximation independent of E .

We have used these parameters to fit Eq. (1) to the rotational diagrams. A fitting is obtained for the following parameter set:

$$g_{\parallel} = 1.95, \quad g_{\perp} = 1.99, \quad D = -2.8 \text{ cm}^{-1},$$

$$E = 0.045 \text{ cm}^{-1}, \quad a = -0.073 \text{ cm}^{-1},$$

but large uncertainties have to be added to E and a . The calculated line positions with these parameters and an exact diagonalization of the SH are given by the lines in Fig. 7.

It is interesting to point out here that besides the resonance lines we have just discussed there are many other small ones that only appear for CrF_3 doped CaF_2 single crystals whose angular dependence cannot be fitted by the SH parameters given above (see for example the white points in Fig. 7). We think that these resonances belong to another chromium defect which is different to $\text{Cr}^{2+}(\text{II})$.

shf structure

The $|+1\rangle \leftrightarrow |-1\rangle$ transitions produce broad and structureless lines for all the studied orientations. In contrast the $|+2\rangle \leftrightarrow |-2\rangle$ transitions consist of five well resolved equally spaced lines with a 1:4:6:4:1 line intensity ratio, the splitting between the lines being almost orientation independent. This structure is due to the shf interaction of the Cr^{2+} $3d$ electron with four equivalent fluoride ions. Taking into account the defect symmetry we propose for this center a model consist-

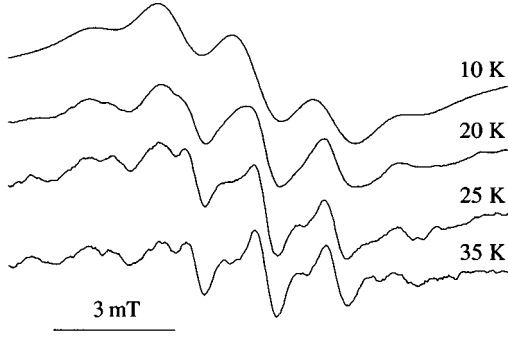


FIG. 8. The temperature dependence for $\text{CaF}_2:\text{Cr}^{2+}(\text{II})$ in the (110) plane at 35° from the [001] direction (9.8 GHz). The intensities have been normalized for presentation purposes.

ing of a Cr^{2+} ion with equally distant fluoride ions in the (110) plane perpendicular to the defect z axis. A similar model has been proposed for Cr^{2+} in $\text{CdF}_2:\text{Cr}$.¹⁶

The shf structure can be explained by adding to the spin Hamiltonian in Eq. (1) the nuclear Hamiltonian in Eq. (6) with i ranging from 1 to 4 and the terms having their usual meaning. Using first order perturbation for the $|\pm 2\rangle$ non-Kramers doublet and assuming that for this doublet $\langle S_x \rangle = \langle S_y \rangle = 0$ and $\langle S_z \rangle = \pm 2$, which is nearly true because the fourth degree term of the electronic SH is much smaller than the other terms, then Eq. (6) becomes

$$\hat{H}_{\text{shf}+nz} = \sum_i \{ -g_n \beta_n (H_x I_x^i + H_y I_y^i + H_z I_z^i) + \langle S_z \rangle (A_{zx}^i I_x^i + A_{zy}^i I_y^i + A_{zz}^i I_z^i) \}, \quad (7)$$

with x , y , and z the defect axes. The axes of the shf interaction are x' , y' , and z' , with z' along the $\text{Cr}^{2+}-\text{F}^-$ bonding direction and $x' \parallel z$. The $A^{\text{shf}(\text{II})}$ tensor for this axis system is diagonal with $A_{x'x'} = A_{y'y'} = A_{\perp}^{\text{shf}(\text{II})}$ and $A_{z'z'} = A_{\parallel}^{\text{shf}(\text{II})}$. With this shf axis choice we obtain $A_{zx} = A_{zy} = 0$ and $A_{zz} = A_{\perp}^{\text{shf}(\text{II})}$. Then the eigenvalues of Eq. (7) are

$$\lambda = \pm \{ (A_{\perp}^{\text{shf}(\text{II})} - \frac{1}{2} g_n \beta_n H_z)^2 + (\frac{1}{2} g_n \beta_n)^2 (H_x^2 + H_y^2) \}^{1/2}. \quad (8)$$

Since the nuclear Zeeman contribution is very small for the lines where the shf structure is resolved the measured shf splitting equals $4A_{\perp}^{\text{shf}(\text{II})}$ independent of the magnetic field orientation. This explains the apparent isotropy of the shf structure observed for the $|+2\rangle \leftrightarrow |-2\rangle$ transitions.

From the experiments the $A_{\perp}^{\text{shf}(\text{II})}$ value obtained for this interaction is 43 ± 3 MHz, compared to ≈ 50 MHz for CdF_2 .¹⁶ No values for the shf parameters are given for SrF_2 . No ESE has been detected for $\text{Cr}^{2+}(\text{II})$ centers.

In Fig. 8 we show the temperature evolution of the EPR spectrum measured at 9.8 GHz. As the temperature increases the half-width of the $|+2\rangle \leftrightarrow |-2\rangle$ lines decreases (1.2 mT at 10 K; 0.55 mT at 35 K). As we shall see later this behavior can be interpreted as a narrowing effect associated with defect motions.

IV. DISCUSSION

Two different Cr^{2+} defects have been identified for CaF_2 . Although in both cases the electronic structure corresponds

to that of a d^4 ion in an orthorhombic environment leading to a non-Kramers $|\pm 2\rangle$ doublet as the ground state, the origin of the distortions are different.

For $\text{Cr}^{2+}(\text{I})$ the EPR lines are narrow and well shaped. Transitions between the $|\pm 1\rangle$ doublet and the $|0\rangle$ and $|+1\rangle$ levels can be observed under favorable conditions. Some of the lines can be measured up to 200 K corresponding to unexpectedly large spin-lattice relaxation times.

For $\text{Cr}^{2+}(\text{II})$ the situation is different. Only the resonance for the $|\pm 2\rangle$ doublet is clearly seen. The transitions within the $|\pm 1\rangle$ doublet are very broad. In addition the relaxation times are presumably so short that no spin-echo nor free induction decay is observed. All these facts point towards a much stronger spin-lattice interaction for the $\text{Cr}^{2+}(\text{II})$ system than for $\text{Cr}^{2+}(\text{I})$.

Let us discuss these differences in light of the possible defect models. Since $\text{Cr}^{2+}(\text{I})$ only appears when Cr_2O_3 is used as the doping agent we can in principle suspect that the $\text{Cr}^{2+}(\text{I})$ center involves some oxygen ionic impurities. This assumption is supported by the shf structure that corresponds to a shf interaction of the Cr^{2+} ion with only two fluoride ions placed along the cube edge in the plane containing the C_2 symmetry axis. The point group symmetry for this center is C_{2v} .

Besides the geometrical information we have obtained from the study of the angular dependence of the shf structure we can gain an insight into the defect model by studying the shf interaction parameters. Our measurements give an isotropic shf interaction constant

$$a = \frac{1}{3} (A_{\parallel}^{\text{shf}(\text{I})} + 2A_{\perp}^{\text{shf}(\text{I})}) = +46 \pm 2.5 \text{ MHz} \quad (9)$$

and an anisotropic one

$$b = \frac{1}{3} (A_{\parallel}^{\text{shf}(\text{I})} - A_{\perp}^{\text{shf}(\text{I})}) = +10 \pm 2 \text{ MHz}. \quad (10)$$

Analysis of these values has been done within the frame of the orthogonalized envelope function method¹⁸ using a perturbation scheme in order to obtain the ground terms corresponding to the appropriated C_{2v} orthorhombic symmetry. For this symmetry any of the A_1 , A_2 , or B_2 terms coming from the cubic ${}^5T_{2g}$ can be the ground state.

The isotropic shf interaction constant is given by the well-known formula

$$a = \frac{8\pi}{3} g_e \mu_B g_n \mu_n \frac{1}{2S} \sum_i |\psi_s^i(R_i)|^2, \quad (11)$$

where $\psi_s^i(R_i)$ is the i wave function of the linear combination of atomic orbitals (LCAO) involving the metal terms and the s orbitals of the ligand. The group-overlap integrals contributing to ψ_s^i have been calculated using the Clementi and Roetti atomic wave functions¹⁹ and depend on the metal-ligand distance R_i .

We have only studied the three lowest terms, not considering mixtures with the terms from the cubic 5E_g nor covalency effects. In Fig. 9(a) we plot the calculated a values as a function of R for the three orbitals. Similarly the anisotropic contribution to the shf constant is given by

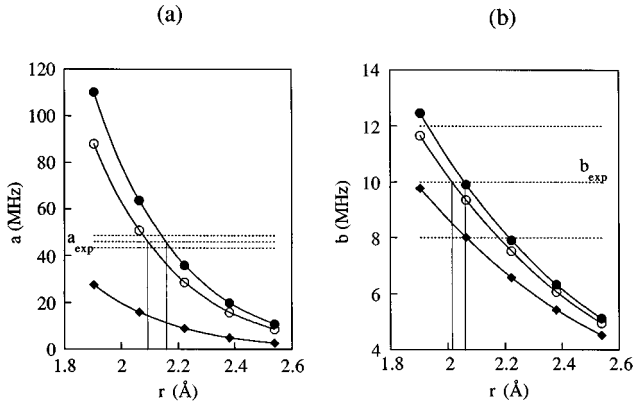


FIG. 9. (a) The isotropic shf constant and (b) the anisotropic shf contribution obtained following the method in the text as a function of the Cr^{2+} - F^- distance. Only the values obtained for the terms coming from the cubic ${}^5T_{2g}$ are represented: \circ : A_1 \bullet : A_2 \blacklozenge : B_2 . The dotted lines correspond to the experimental value obtained for a and b with its error.

$$b = g_e \mu_B g_n \mu_n \frac{1}{4S} \sum_i \int [(3 \cos^2 \theta - 1)/r^3] |\psi_{2p}^i(r)|^2 d\tau + b_{\text{dip}}, \quad (12)$$

where $\psi_{2p}^i(r)$ is the i wave function of the LCAO involving the metal terms and the p orbitals of the ligand and b_{dip} (MHz) = $14.1549 g_n/R^3$ being the dipolar contribution.

In Fig. 9(b) we give the calculated b values as a function of R for the three orbitals. We compare the calculated values with the experimental ones. Best fitting is obtained for a 5A_2 ground term with $R \approx 2.15$ Å compared with the sum of fluorine and chromium ionic radii of ≈ 2.2 Å.

A possible model for this defect is depicted in Fig. 6 and consists of a Cr^{2+} ion displaced along the $[110]$ direction such that it touches the two fluoride ions which are slightly out of their lattice positions. An O^{2-} ion may replace the two opposite F^- ions thus conserving the charge neutrality of the defect. As can be seen in the figure the size of the O^{2-} ion fits in the available site. The remaining four F^- ions may relax outwards which results in a negligible overlapping with the Cr^{2+} electron and explains the absence of any observable shf interaction due to these ions.

The geometrical configuration of this defect is very compact, which may result in large crystal field level splittings and thus in a decrease of the level mixing by the spin-lattice interaction. Such an effect could explain why narrow resonance lines are observed and EPR detection at temperatures relatively high for a non-Kramers doublet is possible. The relative narrow line shapes allow us to determine the ${}^{53}\text{Cr}^{2+}$ hyperfine constants using EPR. They are smaller than for ${}^{53}\text{Cr}^{3+}$ and ${}^{53}\text{Cr}^+$ in the same compound.²⁰

With respect to $\text{Cr}^{2+}(\text{II})$ the experimental evidence is much less complete than for $\text{Cr}^{2+}(\text{I})$. Concerning the geometrical configuration of the defect it is interesting to realize that contrary to $\text{Cr}^{2+}(\text{I})$ we can only resolve the shf structure for the $|+2\rangle \leftrightarrow |-2\rangle$ transition. According to our interpretation of the analysis of this structure we only obtain $A_{\perp}^{\text{shf}(\text{II})}$, thus we do not know if the interaction is isotropic as suggested for the equivalent Cr^{2+} defect in CdF_2 and SrF_2 or

not. In consequence we cannot give a definitive model for this defect, although from the defect symmetry axes we have tentatively proposed it as that for CdF_2 with the fluoride ions placed equidistant from the Cr^{2+} ion in a (110) plane perpendicular to the defect z axis.

The spectra point towards the existence of large inhomogeneous broadening effects due to a distribution of crystal field parameters. In fact the position of the resonance lines within the $|\pm 2\rangle$ doublet are to a first order approximation independent of D and E values. On the contrary, there is a first order zero field splitting proportional to E for the $|\pm 1\rangle$ doublet which explains why the transition lines for the $|\pm 1\rangle$ doublet are wider than for the $|\pm 2\rangle$ one.

Figure 8 shows the temperature evolution of the $|\pm 2\rangle$ line. There is an excess linewidth at 10 K that increases linearly with the magnetic field which can be explained by a parameter distribution. A distribution in D and E values to account for the excess linewidth for the $|\pm 2\rangle$ resonance would produce a broadening of the $|+1\rangle \leftrightarrow |-1\rangle$ transition out of all recognition. Thus we think that the broadening is caused by a distribution of either the g factor, the a term, or the shf interaction parameter, their effect on the linewidth being averaged out by motions induced at high temperatures.

Now an important question arises concerning the possible origin of the observed distortions. As we have said $\text{Cr}^{2+}(\text{II})$ defects are only observed in CaF_2 crystals doped with CrF_3 . Furthermore the orthorhombic symmetry of the center and the observation of a shf interaction with four equidistant fluoride nuclei coincide with previous observations for chromium doped CdF_2 and SrF_2 crystals but this is not the case for Cr^{2+} ions in BaF_2 and SrCl_2 as their symmetry is tetragonal. In all these cases the defects are not associated with other impurities and a JT effect has been suggested to be the origin of the observed distortions.

Next we shall prove that the distortions observed are compatible with the JT effect. Let us consider a cluster consisting of a Cr^{2+} ion in the O_h fluorite cation site surrounded by eight fluoride ions in a cubic symmetry. As we have stated previously, the electronic ground state of the metal ion is ${}^5T_{2g}$. The JT effect couples this level with the e_g and t_{2g} cluster modes. The symmetrized displacements of the atoms in a cubic complex ML_8 for the e_g and the t_{2g} modes used in this discussion are given by Liehr.²¹ The analysis of the $T \otimes (e + 2t_2)$ problem for a tetrahedral complex has recently been studied by Kirk *et al.*²² The form of the interaction is exactly the same for the cubic cluster and their conclusions can be applied to the case reported here.²³

If coupling to e_g modes is dominant, three minima in the Q space corresponding to tetragonal distortions are obtained and the displacements are combinations of modes Q_2 and Q_3 .²⁴ Strains in the e symmetry can stabilize the system in one of the tetragonal distortions and thus the EPR spectra show narrow resonance lines and their angular evolution can be interpreted by an axially symmetric spin Hamiltonian with its axis along the $[100]$ crystal directions (point symmetry D_{4h}).²⁵ This is the case for Cr^{2+} in BaF_2 and SrCl_2 . If coupling to the t_g modes dominates, four trigonal minima are obtained corresponding to linear combinations of the t_g modes. This is the situation for Cr^{3+} ions in CaF_2 and SrF_2 .²⁰

For Cr^{2+} in CaF_2 , CdF_2 , and SrF_2 the EPR spectra can be interpreted by an orthorhombic spin Hamiltonian with small

orthorhombic terms. Coupling to both t_g and e_g modes can indeed produce orthorhombic distortions under certain conditions of quadratic coupling²⁴ and the minima correspond to environments with four equidistant ions in the (110) planes.

It is interesting to note that one of the t_{2g} cube modes is radial whereas the e_g and the other t_{2g} are transverse; it is expected that they will couple to the ion with different strengths. It is also probable that stronger coupling to $Q_4 + Q_5 + Q_6$ modes will exist for CaF_2 , CdF_2 , and SrF_2 than for BaF_2 and SrCl_2 because of the differing lattice distances. This also applies to Cr^{3+} where a preliminary study of BaF_2 indicates a tetragonal instead of the trigonal distortions observed in CaF_2 and SrF_2 .

We will now comment on the SH we have used to interpret the EPR data. A detailed dynamic JT model has been developed by Abhvani *et al.*²⁵ for the tetragonal $\text{GaAs}:\text{Cr}^{2+}$ system and by Parker *et al.*²⁶ for the orthorhombic $\text{GaAs}:\text{Cr}^{3+}$ system.

The JT model involves the derivation of an effective Hamiltonian for the vibronic ground states of the system as well as the calculation of the reduction factors. If appropriate random strains are included, the motion is confined to a potential well as has been studied in detail for the $T_2 \otimes e$ coupling.²⁵ In this case the lowest states are orbital singlets with a small degree of mixing with $l=1$ states caused by the dynamic JT effect and the use of conventional spin Hamiltonian to study the EPR of ground states is therefore fully justified.²⁷

The existence of these stabilizing random strains may also explain the observed distribution in the SH parameters. Furthermore, such a stabilization may be necessary in order to detect JT distorted Cr^{2+} EPR signals. In fact, due to the large anisotropic contributions to the Cr^{2+} SH terms, any dynamical effect associated to jumps between JT potential wells would broaden the lines out of all recognition.

V. CONCLUSIONS

We have identified two orthorhombic Cr^{2+} defects in chromium doped CaF_2 single crystals. The $\text{Cr}^{2+}(\text{I})$ defect is presumably associated with oxygen impurities introduced during doping with the Cr_2O_3 salt. Its shf structure and ESEEM has been fully explained by the interaction with two nearest-neighbor fluoride nuclei. The hf interaction of the $^{53}\text{Cr}^{2+}$ isotope has been resolved.

$\text{Cr}^{2+}(\text{II})$ defects observed for CrF_3 doped CaF_2 possess some properties that may correspond to those of a random strain stabilized JT system. A shf interaction with four nearest-neighbor fluoride ions is observed in this case.

ACKNOWLEDGMENTS

This research was sponsored by CICYT and DGICYT under Contracts No. MAT-92-1279 and No. PB 92-0040. One of us, P.B.O., thanks DGA-CONAI for a grant.

¹The *Dynamical Jahn-Teller Effect in Localized Systems*, edited by Yu. E. Perlin and M. Wagner (North-Holland, Amsterdam, 1984).

²H. A. Jahn and E. Teller, Proc. R. Soc. London Ser. A **161**, 220 (1937).

³J. H. Van Vleck, J. Chem. Phys. **7**, 72 (1939).

⁴U. Opik and M. H. L. Pryce, Proc. R. Soc. London Ser. A **238**, 425 (1957).

⁵J. T. Vallin and G. D. Watkins, Phys. Rev. B **9**, 2051 (1974).

⁶R. Jablonski, M. Domanska, B. Krukowska-Fulde, and T. Nievynski, Mater. Res. Bull. **8**, 749 (1973).

⁷M. M. Zaripov, V. F. Tarasov, V. A. Ulanov, G. S. Shakurov, and M. L. Popov, Phys. Solid State **37** (3), 437 (1995).

⁸M. Bacci, A. Ranfagni, M. Fontana, and G. Viliani, Phys. Rev. B **11**, 3052 (1975); **12**, 5907 (1975).

⁹N. Sakamoto, Phys. Rev. B **26**, 6438 (1982).

¹⁰S. Estreicher and T. L. Estle, Phys. Rev. B **31**, 5616 (1985).

¹¹W. Gelhoff and W. Ulrici, Phys. Status Solidi B **102**, 11 (1980).

¹²P. B. Olivete, V. M. Orera, and P. J. Alonso (unpublished).

¹³J. M. Baker, W. Hayes, and D. A. Jones, Proc. Phys. Soc. **73**, 943 (1959).

¹⁴Notice that the actual states are a combination of $|M_s\rangle$ states. For presentation purposes we will keep the high field labeling for the states.

¹⁵G. H. Stauss, J. J. Krebs, and R. L. Henry, Phys. Rev. B **16**, 974 (1977).

¹⁶R. Jablonski, Mater. Res. Bull. **8**, 909 (1973).

¹⁷A. Schweiger, Angew. Chem. Int. Ed. Engl. **30**, 265 (1991).

¹⁸J. M. Spaeth, J. R. Niklas, and R. H. Bartram, *Structural Analysis of Point Defects in Solids*, Springer Series in Solid-State Sciences Vol. 43 (Springer-Verlag, Berlin, 1992).

¹⁹E. Clementi and C. Roetti, At. Data Nucl. Data Tables **14**, 177 (1974).

²⁰R. Alcalá, P. J. Alonso, V. M. Orera, and H. W. den Hartog, Phys. Rev. B **32**, 4158 (1985).

²¹A. D. Liehr, J. Phys. Chem. **67**, 389 (1963).

²²P. J. Kirk, C. A. Bates, and J. L. Dunn, J. Phys. Condens. Matter **6**, 5465 (1994).

²³C. A. Bates, Phys. Rep. **35**, 187 (1978).

²⁴C. A. Bates, J. L. Dunn, and E. Sigmund, J. Phys. C **20**, 1965 (1987).

²⁵A. S. Abhvani, S. P. Austen, C. A. Bates, L. W. Parker, and D. R. Pooler, J. Phys. C **15**, 2217 (1982).

²⁶L. W. Parker, C. A. Bates, J. L. Dunn, A. Vasson, and A. M. Vasson, J. Phys. Condens. Matter **2**, 284 (1990).

²⁷A. S. Abhvani, C. A. Bates, and D. R. Pooler, J. Phys. C **17**, 1713 (1984).